Electrostatic switch of magnetic core-shell in 0-3 type LSMO/PZT composite film*

Bo Chen(陈波)[1,†], Zi-Run Li(李滋润)[1], Chuan-Fu Huang(黄传甫)[2], and Yong-Mei Zhang(张永梅)[1]

[1] *Department of Physics, School of Science, North University of China, Taiyuan* 030051, *China*
[2] *School of Physics, China University of Mining and Technology, Xuzhou* 221116, *China*

(Received 7 April 2020; revised manuscript received 15 July 2020; accepted manuscript online 1 August 2020)

By dispersing $La_{1-x}Sr_xMnO_3$ (LSMO) granule into $PbZr_xTi_{1-x}O_3$ (PZT) matrix, the 0-3 type LSMO/PZT composite film is synthesized through chemical solution method. The asymmetry of the top and bottom electrodes introduces novel electrostatic screening on LSMO/PZT interface. As electric polarization is switched between upward and downward orientations, the evolution of exchange bias, diode transport, and magnetoresistance is observed. The result implies the electrostatic switch of magnetic core-shell in the present film. In detail, as the spontaneous polarization is upward or downward in the PZT matrix, the ferromagnetic/antiferromagnetic or ferromagnetic/ferromagnetic core-shell structure is formed in LSMO granule, respectively. This work would develop a novel device for spintronics and metamaterial.

Keywords: electric polarization, magnetic core-shell, exchange bias, conductance

PACS: 77.22.Ej, 75.75.Fk, 75.30.Et, 73.50.Jt **DOI:** 10.1088/1674-1056/abab73

1. Introduction

The magnetic core-shell, in which the core and shell display different magnetic orders, is widely and deeply studied now. The exchange bias is notable on the core-shell interface, which results in the shift of the coercive field or remanent magnetization in the hysteresis loop.[1–3] Furthermore, magnetic transport is remarkably influenced by the magnetic shell.[4,5] Up to now, the magnetic core-shell is usually obtained by two methods. The one is modifying the magnetic granule surface with a chemical reaction. For example, by oxidizing the Fe or Co granule surface, the Fe/Fe_2O_3 or Co/CoO core-shell will be formed.[6–8] The other method is embedding the magnetic granule into another magnetic matrix. For example, by mill and segregation procedure, the $NiFe_2O_4$/FeO core-shell will be formed.[1,2] As the magnetic core, the iron-group metal or ferrite usually displays ferromagnetism or ferrimagnetism, respectively. Meanwhile, the oxide shell is usually antiferromagnetic. Most of the magnetic core-shell is invariable after being fabricated.

To explore a novel device for spintronics and metamaterial, the electrostatic switch of the magnetic core-shell is needed.[9,10] As an advantage, the electrostatic switch could be achieved with lower energy and higher speed. This goal may be realized in the 0-3 type LSMO/PZT composite film, which is comprised of $La_{1-x}Sr_xMnO_3$ (LSMO) granule and $PbZr_xTi_{1-x}O_3$ (PZT) matrix. Taking the metal and oxide layers as top and bottom electrodes respectively, the electrostatic screening becomes asymmetric across the composite film.[11] Furthermore, because the LSMO manganite displays metallic ferromagnetism,[12] the coupling between electrostatic screening and magnetic order may occur on LSMO/PZT interface.

Such a coupling mechanism is possible according to our recent work.[11] As the electric polarization is downward or upward in the PZT matrix, the electron is accumulated or depleted on LSMO granule surface, respectively. Due to the competition between double-exchange and super-exchange interactions, the magnetic ground state is variable in LSMO crystal. As the electron is accumulated or depleted, the LSMO granule surface prefers ferromagnetism or antiferromagnetism respectively.[13–15] However, because the electrostatic screening depth is no more than 1.0 nm, the intrinsic ferromagnetism is retained in LSMO granule core.[16] Thus, the ferromagnetic/ferromagnetic (FM/FM) or ferromagnetic/antiferromagnetic (FM/AFM) core-shell structure would be formed in LSMO granule. The electric polarization can be switched by the electrostatic field, and the remnant polarization can be held in the PZT matrix. As a result, such an electrostatic switch of magnetic core-shell would be reversible and nonvolatile.[17]

In this work, the 0-3 type LSMO/PZT composite film is fabricated through chemical solution deposition. The platinum (Pt) and indium tin oxide (ITO) layers are taken as top and bottom electrodes, respectively. As the electric polarization is upward or downward, both the magnetic response and magnetic

*Project supported by the Science Foundation of North University of China (Grant No. 2017026), the Applied Basic Research Foundation of Shanxi Province, China (Grant No. 201801D221143), the Scientific and Technological Innovation Programs of Higher Education Institutions in Shanxi, China (Grant No. 2019L0535), and the National Natural Science Foundation of China (Grant No. 11847012).

†Corresponding author. E-mail: BoChen@nuc.edu.cn

transport are investigated. This work achieves the electrostatic switch of magnetic core-shell.

2. Method

Through solving $Pb(CH_3COO)_2$, $Zr(NO_3)_4$, and $Ti(C_4H_9O)_4$ into 2-methoxyethanol, the PZT precursor is produced. Through solving $La(CH_3COO)_3$, $Sr(CH_3COO)_2$, and $Mn(CH_3COO)_2$ into n-octyl ether, baking the solution, and sintering the powder, the LSMO granule is produced. To obtain the optimal ferroelectric and ferromagnetic property, the Zr/Ti and La/Sr ratio is selected as 0.2/0.8 and 0.7/0.3, respectively.[12,18] Then, the LSMO granule is dispersed into the PZT precursor by ultrasonic vibration. Through depositing the mixed solution on ITO/glass substrate by coating technique, and annealing the deposited layer under an oxygen atmosphere, the 0-3 type LSMO/PZT composite film is obtained. Finally, the Pt layer is grown on the top surface by the sputtering method. The fabrication procedure is seen in Fig. 1(a). For the present film, the crystalline phase is characterized by x-ray diffraction (XRD) with Cu K_α radiation. The cross-section morphology is observed by both scanning electron microscopy (SEM) and transmission electron microscopy (TEM). Furthermore, the magnetic force microscopy (MFM) is applied to investigate the distribution of LSMO granule in the PZT matrix.

The ferroelectric hysteresis is measured on the standard ferroelectric test unit. Both the magnetic response and magnetic transport are investigated on the physical property measurement system (PPMS). During the magnetic response measurement, the cooling field is set as 0 kOe and 10 kOe sequentially, meanwhile the pulse voltage is set as -9 V, 0 V, and $+9$ V sequentially. The composite film is cooled from 300 K to 5 K under each cooling field and pulse voltage. Then the magnetic hysteresis loop is measured at 5 K. The magnetic transport measurement is carried at room temperature. Firstly, the -9 V or $+9$ V pulse is applied to switch the spontaneous polarization. Then, the direct voltage is swept from -1 V to $+1$ V, meanwhile, the electric current across the top and bottom electrodes is detected. The sweep and detection are cycled four times, when the magnetic field of 0.0 kOe, 0.5 kOe, 1.0 kOe, and 1.5 kOe is applied sequentially.

In the present film, the bottom electrode is defined as zero potential plane, thus the spontaneous polarization is upward and downward under -9 V and $+9$ V pulse, respectively. After 10 kOe cooling, the pulse dependence of the magnetic response is investigated. At 5 K, the pulse voltage is swept in four ways, i.e., -9 V to $+9$ V, $+9$ V to -9 V, 0 V to $+9$ V, and 0 V to -9 V. During all the sweeps, the magnetic hysteresis loop is measured immediately after each pulse. At room temperature, the pulse dependence of magnetic transport is also investigated. In detail, the magnetic field of 1.00 kOe, 1.25 kOe, and 1.50 kOe is applied to the film sequentially. Under each magnetic field, the pulse voltage is swept in two ways, i.e., -9 V to $+9$ V and $+9$ V to -9 V. During all the sweeps, the current is detected after each pulse, with measuring voltages of both $+1$ V and -1 V.

3. Result and discussion

3.1. Morphology

In Fig. 1(b), the SEM image shows each compact layer and distinct interface. The thickness of the Pt, LSMO/PZT, and ITO layer is estimated as 30 nm, 100 nm, and 60 nm, respectively. According to Fig. 1(c), the TEM image shows LSMO granule is dispersed in the PZT matrix, and the LSMO granule is isolated along the thickness direction. Furthermore, the LSMO granule diameter is estimated as 20 nm. In Fig. 2(a), only the XRD peak of perovskite LSMO, perovskite PZT, and bixbyite ITO phase is observed.[19] No peak of the impurity phase is found in the XRD spectrum. Here the XRD measurement is carried without the Pt layer, because the peak of the Pt and PZT would cover each other. After the LSMO granule is magnetized upward or downward, the observed MFM image is shown in Fig. 2(b) or Fig. 2(c), respectively. The bright and dark colors imply repulsive and attractive forces on probe respectively.[20] Because the probe is magnetized downward permanently, the bright and dark regions represent upward and downward magnetizations of the LSMO granule, respectively. It further proves that the ferromagnetic LSMO granule is dispersed in a nonmagnetic PZT matrix.

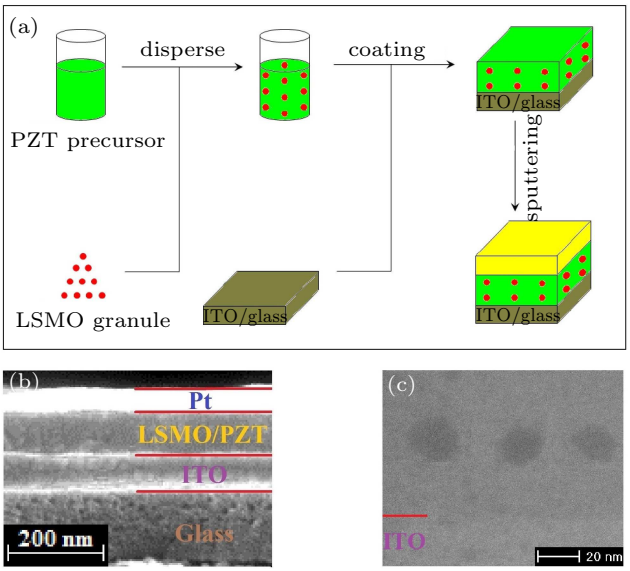

Fig. 1. (a) The fabrication procedure. (b) The cross-section SEM image. (c) The cross-section TEM image of 0-3 type LSMO/PZT composite film.

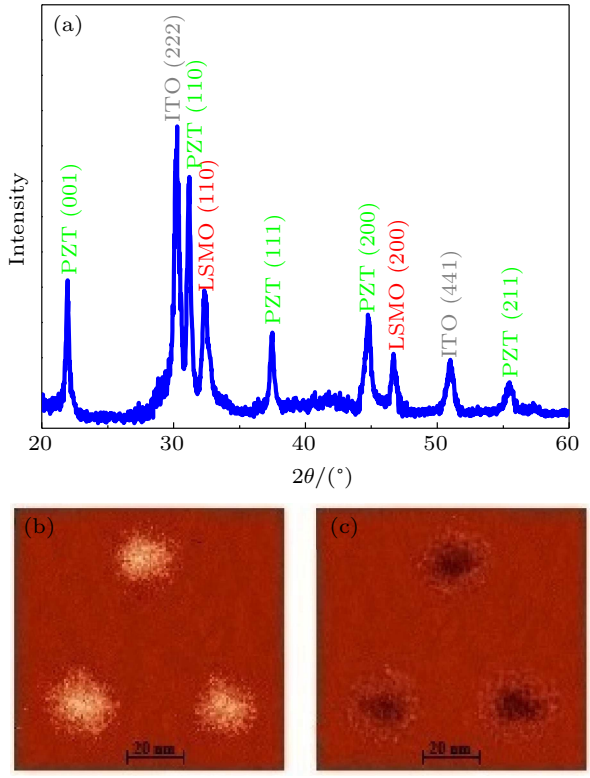

Fig. 2. (a) The XRD spectrum. (b), (c) The MFM image observed after upward and downward magnetizing of the LSMO granule, respectively.

3.2. Exchange bias

The ferroelectric loop is plotted in Fig. 3(a). At the saturated voltage of 9 V, the coercive voltage and remnant polarization reach 2 V and 37.5 μC/cm^2, respectively. During the standard ferroelectric measurement, the voltage sweep is 0 V to +9 V, +9 V to −9 V, and −9 V to 0 V successively. At the initial and final moments, the PZT matrix is incompletely and completely polarized, respectively. Thus, the polarization gap at 0 V is present in the ferroelectric loop. For magnetic response measurement, the 10 kOe and 0 kOe cooling loops are plotted in Figs. 3(b) and 3(c) respectively. To clarify the exchange bias behavior, the hysteresis loop is amplified between ±1.5 kOe.[21] As spontaneous polarization rotates from downward to upward orientation, i.e., the pulse voltage is altered from +9 V to −9 V, the 10 kOe cooling loop is negatively biased in Fig. 3(b). Under −9 V, 0 V, and +9 V pulses, the positive coercive fields are about +120 Oe, +170 Oe, and +190 Oe, respectively, meanwhile, the negative coercive field are about −280 Oe, −220 Oe, and −190 Oe, respectively. However, the case is very different for the 0 kOe cooling loop. Under −9 V, 0 V, and +9 V pulses, the coercive fields in Fig. 3(c) are about ±240 Oe, ±190 Oe, and ±180 Oe, respectively. Here, as the spontaneous polarization rotates from downward to upward orientation, the coercive field is only increased in amplitude, while the bias behavior is absent.

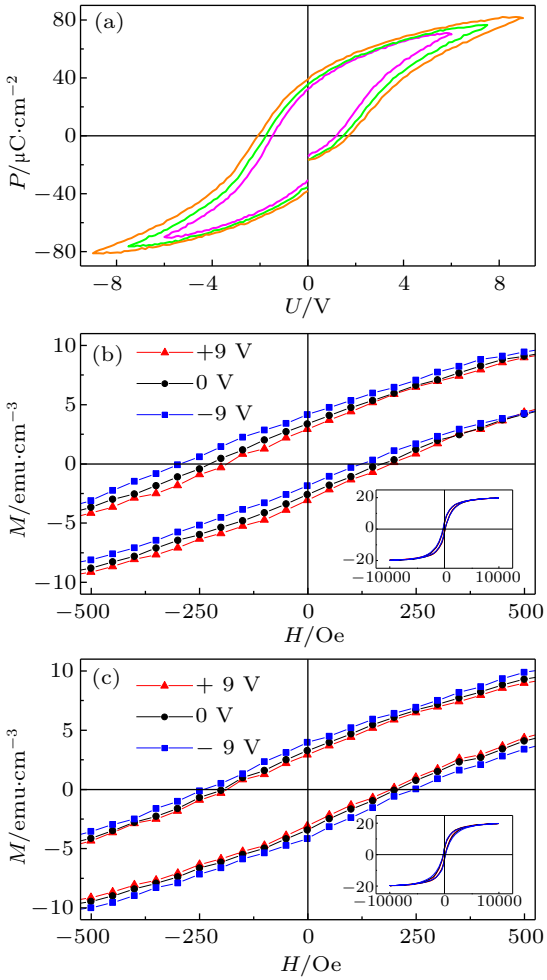

Fig. 3. (a) The ferroelectric hysteresis loop. (b), (c) The amplification of magnetic hysteresis loop for 10 kOe and 0 kOe cooling, respectively. The complete magnetic loop is in the insert.

In the present film, the electrostatic screening depths of the LSMO granule, the Pt electrode, and ITO electrodes are about 1.0 nm, 0.05 nm, and 0.65 nm, respectively.[16,22,23] According to the SEM and TEM images, the thickness of the PZT matrix is about 100 nm, and the diameter of the LSMO granule is about 20 nm. Taking these parameters into our previous model, the electric polarization in the composite film is simulated numerically.[11,24] As illustrated in Figs. 4(b) and 4(c), the electric polarization near the LSMO/PZT interface deviates the spontaneous polarization. Accompanying the upward or downward polarization, the electron is depleted or accumulated on the LSMO granule surface, respectively.[11,24] More explanation is in our previous work.

In the LSMO crystal, the double exchange and superexchange prefer ferromagnetic and antiferromagnetic order, respectively. For the present La/Sr ratio, the double exchange is dominant, and the LSMO granule displays ferromagnetism.[12] As the electron is depleted or accumulated on the LSMO granule surface, the superexchange or double exchange is enhanced. The ferromagnetic-to-antiferromagnetic transition occurs in the former case, while the ferromagnetic order is retained in the latter case.[13–15]

Because the electrostatic screening depth is no more than 1.0 nm, the intrinsic ferromagnetic order is retained inside LSMO granule.[16] Thus, as the spontaneous polarization is upward and downward in the PZT matrix, the FM/AFM and FM/FM core-shell structures are formed in LSMO granule, respectively. The coupling between electric polarization and magnetic core-shell is explicitly illustrated in Figs. 4(b) and 4(c).

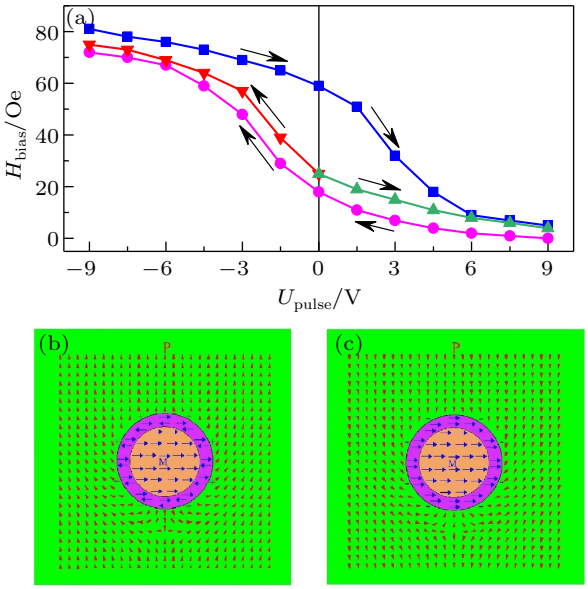

Fig. 4. (a) The pulse dependence of the bias field. (b), (c) The magnetic core-shell coupling with upward and downward polarization, respectively.

In the FM/AFM core-shell structure, certain exchange interaction exists between antiferromagnetic shell and ferromagnetic core. After 10 kOe cooling, the magnetic moment near the core-shell interface is parallel with the cooling field. During the hysteresis measurement, as the core moment is parallel or antiparallel with the adjacent shell moment, the exchange interaction prevents or promotes the ferromagnetic rotation.[1–3] Thus, the coercive field is negatively biased in Fig. 3(b), as observed in other LSMO granules.[25] However, after 0 kOe cooling, the magnetic moment randomly orientates near the core-shell interface. Here, the disordered exchange interaction always pins the ferromagnetic rotation.[1–3] Thus, the amplitude of the coercive field is increased in Fig. 3(c).

In the FM/FM core-shell structure, the magnetic moment of core and shell simultaneously rotates with the external magnetic field. Thus, both the bias and enhancement of the coercive field disappear, as seen in Figs. 3(b) and 3(c). Under 0 V pulse, the PZT matrix is depolarized, and the electrostatic screening is negligible on the LSMO granule surface. However, due to the broken or incomplete chemical bond, the spin-glass order exists on the LSMO granule surface.[26] Here, weak exchange interaction still occurs between the spin-glass shell and ferromagnetic core, which results in the slight bias and enhancement of the coercive field under 0 V pulse, as seen in Figs. 3(b) and 3(c).[25] In a word, under −9 V, 0 V, and +9 V pulses, the antiferromagnetic, spin-glass, and ferromagnetic orders are formed on the LSMO granule surface, respectively.

As seen in the above, the electrostatic switch of magnetic core-shell is achieved in the present film, which is further proved in Fig. 4(a). Here the bias field is defined as $H_{\rm bias} = |H_+ + H_-|/2$. The H_+ and H_- represent the positive and negative coercive fields, respectively, which are extracted from the hysteresis loop measured after each pulse. The measurement method is described in Section 2. As pulse voltage is swept between ±9 V, the hysteresis evolution of the bias field is consistent with the ferroelectric hysteresis in Fig. 3(a). Under −9 V and +9 V pulses, the bias field reaches the maximum and minimum, respectively. Near ±3 V pulse, the bias field is switched between two extrema. Furthermore, as pulse voltage is only swept from 0 V to −9 V or +9 V, the bias field also tends to the maximum or minimum. Thus, the electrostatic switch of the magnetic core-shell is nonvolatile and reversible in the present film.

3.3. Transport behavior

For −9 V and +9 V pulses, the current–voltage curves are plotted in Figs. 5(a) and 5(b), respectively. Accompanying upward and downward polarization, the electrostatic screening potential is negative and positive in the PZT matrix, respectively. During the measurement, as the screening potential is toward or backward to the external potential, the electrostatic field is enhanced or weakened. Thus, diode transport is obvious in both Figs. 5(a) and 5(b), which means the current amplitude is asymmetric between positive and negative voltages. Besides, accompanying upward or downward polarization, the depletion or accumulation of electron makes the Fermi level is lower or higher on LSMO granule surface. In the two cases, the Fermi level labeled as E_+ and E_-, respectively. As electron hops among adjacent LSMO granules, the hopping probability is inversely correlative with the barrier height, i.e., $E_0 - E_+$ and $E_0 - E_-$ in Figs. 5(c) and 5(d), respectively. Thus, for −9 V and +9 V pulses, the average current amplitude is different from each other, as seen in Figs. 5(a) and 5(b).

In Fig. 5(a) and 5(b), the current increases with the magnetic field monotonously. For −9 V and +9 V pulses, the magnetoresistance (MR) ratios at 1.5 kOe are estimated as 10% and 60%, respectively. Such pulse dependence of MR also implies the electrostatic switch of magnetic core-shell. As electron hops among adjacent LSMO granules, the hopping probability is influenced by the scattering from the granule surface. Accompanying upward or downward polarization, the LSMO granule surface displays antiferromagnetism or ferromagnetism, respectively. In the former case, the scattering from the antiferromagnetic surface is stronger. In the latter

case, as the ferromagnetic moment gradually orientates to the external field, the surface scattering becomes weaker.[27] Thus, lower or higher MR ratio is observed with upward or downward polarization. The coupling between electric polarization and magnetic transport is explicitly illustrated in Figs. 5(c) and 5(d).

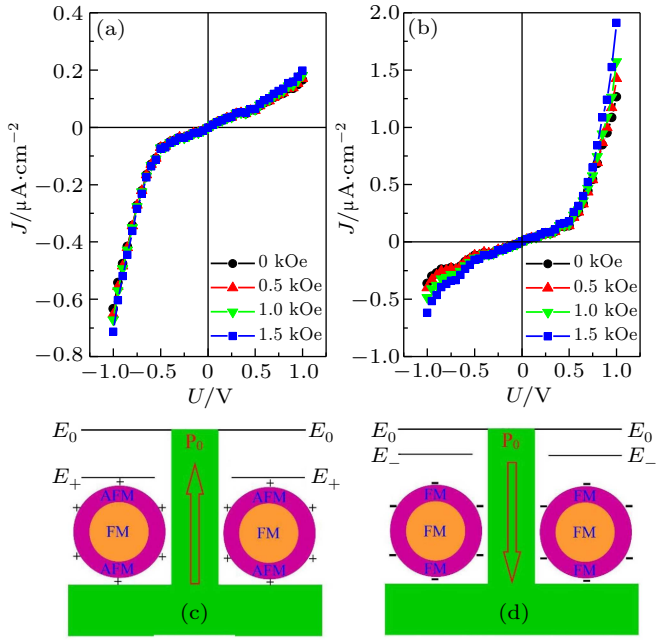

Fig. 5. (a), (b) The current–voltage curve measured after −9 V and +9 V pulse, respectively. (c), (d) The hopping mechanism for upward and downward polarization, respectively.

The pulse dependence of diode ratio and MR ratio is plotted in Fig. 6. Here the diode ratio is defined as I_-/I_+, where the currents I_+ and I_- are detected at the direct voltages of +1 V and −1 V, respectively. The MR ratio is defined as $(\Delta I_+/I_+ + \Delta I_-/I_-)/2$, where ΔI_+ and ΔI_- represent the currents altered by the magnetic field. As pulse voltage is swept between ±9 V, the hysteresis evolution of both diode ratio and MR ratio is obvious. The highest diode and lowest MR ratio are reached under −9 V pulse, while the lowest diode and highest MR ratio are reached under +9 V pulse. Near ±3 V pulse, both the diode and MR ratio are switched between two extrema. All the behavior is consistent with not only the magnetic transport mechanism in Figs. 5(c) and 5(d), but also the ferroelectric hysteresis in Fig. 3(a). Thus, the electrostatic switch of the magnetic core-shell is nonvolatile and reversible in the present film.

This work would achieve the electric-write device. In detail, the upward and downward polarizations of the PZT matrix represent "1" and "0" bits, respectively, which is written by electrostatic voltage. The "1" and "0" bits are accompanied by FM/AFM and FM/FM core-shell, respectively. Through detecting the diode ratio or MR ratio, the bit could be readout. Comparing to the magnetic-write way in the rigid disk, the electric-write way could be achieved with higher speed and lower energy.

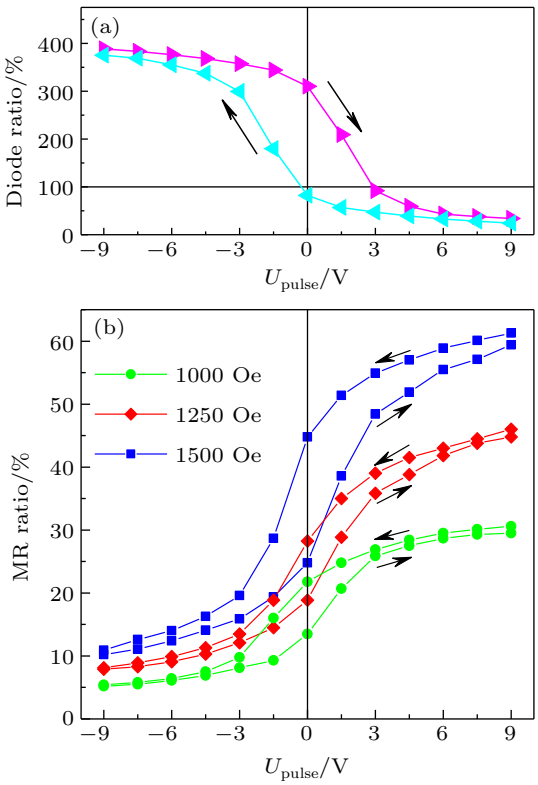

Fig. 6. The pulse dependence of (a) diode ratio and (b) MR ratio.

4. Conclusion

In this work, the 0-3 type LSMO/PZT composite film is fabricated through chemical solution deposition. As spontaneous polarization rotates from downward to upward orientation, the negative bias of the coercive field is observed after 10 kOe cooling, while an increase of the coercive field is observed after 0 kOe cooling. The upward or downward polarization results in lower or higher MR ratio. Besides, diode transport is observed in the present film. These results imply the electrostatic switch of magnetic core-shell in the 0-3 type LSMO/PZT composite film. As pulse voltage is swept, all the hysteresis evolutions of bias field, diode ratio, and MR ratio are obvious. Thus, the electrostatic switch of the magnetic core-shell is nonvolatile and reversible.

The recent work predicts the elastic field could induce spin transition in the magnetic core-shell structure.[28] This work achieves the switch of magnetic core-shell by the electrostatic field. It is a new method to manipulate the magnetic core-shell. Furthermore, in the ZnSe/ZnS core-shell structure, the electrostatic switch of resistance is achieved recently.[29] In this work, the resistance responds to both electrostatic and magnetic fields, i.e., the diode and MR transport, respectively. It reveals the multi-field response of the magnetic core-shell structure.

References

[1] Noguesa J, Sorta J, Langlaisb V, Skumryeva V, Surinachb S, Munozb J S and Barob M D 2005 *Phys. Rep.* **422** 65

[2] Manna P K and Yusuf S M 2014 *Phys. Rep.* **535** 61

[3] Markovich V, Puzniak R, Fita I, Mogilyansky D, Wisniewski A, Gorodetsky G and Jung G 2014 *J. Phys. Chem. C* **118** 7721

[4] Huang Z G, Chen Z G, Peng K, Wang D H, Zhang F M, Zhang W Y and Du Y W 2004 *Phys. Rev. B* **69** 094420

[5] Jirak Z, Hirschner J, Kaman O, Knizek K, Levinsky P, Marysko M and Hejtmanek J. 2017 *J. Phys. D: Appl. Phys.* **50** 075001

[6] Khurshid H, Phan M H, Mukherjee P and Srikanth H 2014 *Appl. Phys. Lett.* **104** 072407

[7] Ge C N, Wan X G, Eric P, Hu Z W, Wen I L, Michael B, Zou W Q and Du Y W 2015 *Chin. Phys. B* **24** 034501

[8] Nieves P, Kechrakos D and Fesenko O C 2016 *Phys. Rev. B* **93** 064432

[9] Feng J N, Liu W, Geng D Y, Ma S, Yu T, Zhao X T, Dai Z M, Zhao X G and Zhang Z D 2014 *Chin. Phys. B* **23** 087503

[10] Hyun B R, Marus M, Zhong H Y, Li D P, Liu H C, Xie Y, Koh W K, Xu B, Liu Y J and Sun X W 2020 *Chin. Phys. B* **29** 018503

[11] Chen B, Pan D F, Duan M L and An P L 2019 *Phys. Rev. B* **100** 134418

[12] Salamon M B and Jaime M 2001 *Rev. Mod. Phys.* **73** 583

[13] Vaz C A F, Segal Y, Hoffman J, Grober R D, Walker F J and Ahn C H 2010 *Appl. Phys. Lett.* **97** 042506

[14] Dong S, Zhang X T, Yu R, Liu J M and Dagotto E 2011 *Phys. Rev. B* **84** 155117

[15] Leufke P M, Kruk R, Brand R A and Hahn H 2013 *Phys. Rev. B* **87** 094416

[16] Hong X, Posadas A and Ahn C H 2005 *Appl. Phys. Lett.* **86** 142501

[17] Glazkova E, McCash K, Chang C M, Mani B K and Ponomareva I 2014 *Appl. Phys. Lett.* **104** 012909

[18] Kukhar V G, Pertsev N A, Kohlstedt H and Waser R 2006 *Phys. Rev. B* **73** 214103

[19] Pan D F, Bi G F, Chen G Y, Zhang H, Liu J M Wang G H and Wan J G 2016 *Sci. Rep.* **6** 22948

[20] Gao X S, Rodriguez B J, Liu L F, Birajdar B, Pantel D, Ziese M, Alexe M and Hesse D 2010 *ACS Nano* **4** 1099

[21] Rajagopal R, Mona J, Kale S N, Bala T, Pasricha R, Poddar P, Sastry M, Prasad B L V, Kundaliya D C and Ogale S B 2006 *Appl. Phys. Lett.* **89** 023107

[22] Ma Z J, Chen G, Zhou P, Mei Z H and Zhang T J 2017 *J. Phys. D: Appl. Phys.* **50** 015303

[23] Xian S L, Nie L X, Qin J, Kang T T, Li C Y, Xie J L, Deng L J and Bi L 2019 *Opt. Express* **27** 28618

[24] Chen B, Su N N, Cui W L and Yan S N 2018 *Phys. Lett. A* **382** 1124

[25] Rostamnejadi A, Venkatesan M, Salamati H, Ackland K, Gholizadeh H, Kameli P and Coey J M D 2017 *J. Appl. Phys.* **121** 173902

[26] Nayek C, Samanta S, Manna K, Pokle A, Nanda B R K, Anilkumar P S and Murugavel P 2016 *Phys. Rev. B* **93** 094401

[27] Yang H, Cao Z E, Shen X, Xian T, Feng W J, Jiang J L, Feng Y C, Wei Z Q and Dai J F 2009 *J. Appl. Phys.* **106** 104317

[28] Singh Y, Oubouchou H, Nishino M, Miyashita S and Boukheddaden K 2020 *Phys. Rev. B* **101** 054105

[29] Wang Z P, Wang Y, Yu J B, Yang J Q, Zhou Y, Mao J Y, Wang R P, Zhao X J, Zheng W H and Han S T 2020 *Nano Lett.* **20** 5562